Remote Sensing of Environment 137 (2013) 69–83

Contents lists available at SciVerse ScienceDirect

Remote Sensing of Environment

journal homepage: www.elsevier.com/locate/rse

Validation of GRACE-derived terrestrial water storage from a regional approach over South America

Frédéric Frappart *[,1], Lucía Seoane, Guillaume Ramillien [1]

Université de Toulouse, OMP-GET, UM5563, CNRS/IRD/UPS, 14 Avenue Edouard Belin, 31400 Toulouse, France

ARTICLE INFO

Article history:
Received 18 December 2012
Received in revised form 14 June 2013
Accepted 15 June 2013
Available online 12 July 2013

Keywords:
GRACE
Surface water
Groundwater, water levels
Discharges

ABSTRACT

We propose to validate regional solutions consisting of 2° surface tiles of surface mass concentration over South America (90°W–30°W; 60°S–20°N) computed using accurate Level-1 GRACE measurements, by confronting them to other GRACE products (*i.e.*, global GRGS and ICA-400 km GFZ/CSR/JPL combined solutions) and independent in situ river level and discharge datasets. For this purpose, Principal Component Analysis (PCA) was applied to all of these types of GRACE-based solutions to extract the corresponding main orthogonal spatial and temporal modes of variability to be compared for 2003–2010. For the first three spatial modes, regional solutions provide a better geographical localization of hydrological structures, especially indicating major surface and groundwater systems of South America. Over hydrological patterns, records of river level *versus* time are particularly consistent with the GRACE temporal modes, especially for our regional solutions (*i.e.*, correlations generally greater than 0.7). Interannual variations of GRACE-based Terrestrial Water Storage (TWS) clearly exhibit the signatures of extreme climatic events as the recent droughts and floods that affected South America. Very significant agreement is also found at interannual time-scale between TWS and discharges in drainage basins dominated by the surface reservoir (more than 0.9 of correlation in the Amazon basin).

1. Introduction

Continental water storage is a key component of the global hydrological cycle which plays a major role in the Earth's climate system that controls over water, energy and biogeochemical fluxes. In spite of its importance, the total continental water storage is not well-known at regional and global scales because of the disparity of in situ observations and systematic monitoring of the terrestrial water reservoirs, especially the groundwater component (Alsdorf & Lettenmaier, 2003).

The Gravity Recovery and Climate Experiment (GRACE) mission provides a global mapping of the time-variations of the gravity field at an unprecedented resolution of ~400 km and a centimetric precision in terms of geoid height. Tiny variations of gravity measured by GRACE are mainly due to the redistribution of mass inside the fluid envelops of the Earth (*i.e.*, atmosphere, oceans and continental water storage) from monthly to decadal timescales (Tapley, Bettadpur, Ries, Thompson, & Watkins, 2004).

Since its launch in March 2002, the GRACE terrestrial water storage anomalies have been increasingly used for large-scale hydrological applications (see Ramillien, Famiglietti, Wahr, 2008; Schmidt et al., 2008 for reviews). These studies demonstrated a great potential to monitor extreme hydrological events (Andersen, Seneviratne, Hinderer, & Viterbo, 2005; Chen, Wilson, Tapley, Yang, & Niu, 2009; Frappart, Ramillien, & Ronchail, in press; Seitz, Schmidt, & Shum, 2008), to monitor aquifer storage (Leblanc, Tregoning, Ramillien, Tweed, & Fakes, 2009; Rodell et al., 2007; Strassberg, Scanlon, & Rodell, 2007) and snowpack (Frappart, Ramillien, & Famiglietti, 2011) variations, and to estimate hydrological fluxes, such as basin-scale evapotranspiration rate (Ramillien et al., 2006; Rodell et al., 2004) and discharge (Syed, Famiglietti, & Chambers, 2009).

Unfortunately, GRACE Level-2 solutions suffer from the presence of important north–south striping when determining Stokes coefficients (*i.e.*, spherical harmonics of the geopotential corrected from known gravitational accelerations using a priori models for atmosphere, ocean mass, and tides) which are geophysically unrealistic, and aliasing of short-time phenomena. Because of these effects of striping that limits further interpretation, different post-processing approaches for filtering these residual GRACE geoid solutions have been proposed to extract useful hydrological signals (see Ramillien, Famiglietti, Wahr, 2008; Schmidt et al., 2008 for reviews) with the risk of losing energy in the short wavelength domain, and thus missing details (*i.e.*, loss of resolution).

To overcome this problem, local determination of the time variations of the surface water storage has been developed (Eicker, 2008; Rowlands et al., 2005). They are of great interest for regions where very localized important mass variations occur, such as flood and glacier fields. Mascons consist of adjusting regional heights of individual surface elements by using scaling factors of spherical harmonics. However, they remain equivalent to classical global solutions (Rowlands et al., 2010). Another type of regional approach has been more recently proposed by directly

* Corresponding author. Tel.: +33 5 61 33 29 40.
E-mail addresses: frederic.frappart@gmail.com, frederic.frappart@get.obs-mip.fr (F. Frappart).
[1] Groupe de Recherche en Géodésie Spatiale.

0034-4257/$ – see front matter © 2013 Elsevier Inc. All rights reserved.
http://dx.doi.org/10.1016/j.rse.2013.06.008

adjusting the surface mass density distribution at the surface of the Earth from the Level-1 GRACE data, especially the accurate satellite-to-satellite velocity variations or K-Band Range Rate (KBRR) measurements (Ramillien, Biancale, Gratton, Vasseur, & Bourgogne, 2011), and taking spatial correlations *versus* the geographical distance between juxtaposed surface elements into account (Ramillien et al., 2012).

In particular, power spectral density reveals that the regional solutions computed over South America are more energetic than the bandlimited global Level-2 solutions at short and medium spatial wavelengths (<4000 km) (Ramillien et al., 2012). In the present study, our goal is to demonstrate that the excess of energy present at short wavelengths (between 400 and 1000 km) in the regional solutions compared to the global solutions can be related to realistic geophysical signals corresponding to hydrological events such as floods, melt of glaciers, or groundwater variations. To verify this assumption, a Principal Component Analysis (PCA) was first applied to the GRACE-based regional and global solutions. The resulting spatial and temporal modes were compared to the spatial distribution of surface and ground waters and correlated to water level variations from in situ gauges located close to the mouth of the major river basins and sub-basins of South America respectively. Then, basin-averaged anomalies of TWS from this regional approach are compared with changes of in situ surface water discharges in the largest drainage basins of South America (*i.e.*, Amazon, La Plata, Orinoco, and Tocantins), as well as basin-averaged anomalies of TWS from global GRACE solutions.

To our knowledge, there is no large area in the world covered with a sufficient density of in situ measurements of all the hydrological reservoirs to directly validate GRACE data. Most of the previous studies dealing with the validation of the data present comparisons between GRACE-based TWS and hydrological outputs, and/or comparisons with external hydrological datasets such as gridded rainfall and in situ water levels and discharges (see Ramillien, Famiglietti, Wahr, 2008; Schmidt et al., 2008 for reviews). Here, we have chosen to compare the GRACE-based TWS from our regional approach to other global available solutions and to, according to your opinion, a profound and extensive datasets of in situ water levels. We decided not to compare to hydrological model outputs because most of the hydrological models do not simulate the slow reservoirs such as the floodplains and the groundwater.

2. Datasets & methods

2.1. Water mass variations from GRACE solutions

2.1.1. Constrained regional solutions

An alternative regional approach to the ones based on spherical harmonics has been recently proposed to improve geographical localization of hydrological structures and to reduce leakage and aliasing errors. Our regional approach consists of determining water mass variations over juxtaposed surface elements in a given continental region from GRACE residual potential difference anomalies, in terms of equivalent-water heights. According to the energy integral approach, these latter along-track anomalies correspond mainly to the contribution of the continental hydrology to the gravity field changes measured by GRACE, they are obtained from KBR range velocity differences between the two GRACE satellites after a priori (*i.e.*, de-aliasing) corrections of mass variations occurring in the oceans and the atmosphere, are made by pre-processing of GRACE observations. By assuming the conservation of energy along the GRACE tracks, it consists of recovering equivalent-water thicknesses of juxtaposed 2 by 2-degree geographical tiles by inverting GRACE inter-satellite KBR Range (KBRR) residuals (see Ramillien et al., 2011, 2012). These KBRR residuals were obtained by correcting the raw GRACE observations from the a priori gravitational accelerations of known large-scale mass variations (*i.e.*, atmosphere and oceanic mass variations, polar movements, as well as solid and oceanic tides) during the iterative least-squares orbit adjustment made using the GRGS GINS software (Bruinsma, Lemoine, Biancale, & Valès, 2010; Lemoine et al., 2007). The effects of non-conservative forces measured by on-board GRACE accelerometers are also removed from the along-track observations, in order to extract the contributions of the remaining not modeled phenomena, thus mainly water mass changes in continental hydrology. Since classical gravimetric inversion does not provide a unique solution and to reduce the spurious effects of the noise in the observations, regularization strategies have been proposed to find numerically stable regional solutions, either based on Singular Value Decomposition (SVD) and L-curve analysis (Ramillien et al., 2011), or by introducing spatial constraints (Ramillien et al., 2012). Time series of successive 10-day regional solutions of water mass have been produced over the whole South America (90°W–30°W; 60°S–20°N) following this regional approach for 2002–2010, and these 2°-by-2° maps revealed realistic amplitudes, for spatial wavelengths lesser than the dimensions of the region itself by construction (*i.e.*, <6500–8000 km, or equivalently harmonic degrees less than 5–6 for South America). Numerical estimations show us that the predicted regional solutions need to be completed by long wavelength components before being compared with other data sets, when the geographical region is not large enough to contain these long gravity undulations. Over South America, we complemented each regional solution with short and medium wavelengths up to degree 5 from the corresponding GRGS solution (for more details see Ramillien et al., 2012).

2.1.2. ICA-filtered solutions

A post-processing method based on Independent Component Analysis (ICA) was applied to the Level-2 GRACE solutions from different official providers (*i.e.*, UTCSR, JPL and GFZ), after pre-filtering with 400-km-radius Gaussian filters. This approach does not require any a priori information, except the assumption of statistical independence between the elementary sources that compose the measured signals (*i.e.*, useful geophysical signals plus noise). Separation consists of finding the independent sources by solving a linear system relating the GRACE solutions provided for a given month, to the unknown independent components. The contributors to the observed gravity field are forced to be uncorrelated numerically by imposing diagonal cross-correlation matrices. For a given month, the ICA-filtered solutions only differ to each other from a scaling factor, so that the GFZ-derived ICA-filtered solutions are only considered. The efficiency of the ICA in separating gravity signals from noise by combining Level-2 GRACE solutions has previously been demonstrated over land (Frappart, Ramillien, Maisongrande, & Bonnet, 2010; Frappart, Ramillien, Leblanc, et al., 2011) and ice caps (Bergmann, Ramillien, & Frappart, 2012). These monthly ICA solutions are available at: http://grgs.obs-mip.fr. They correspond to what is referred to the first ICA mode (whereas the second and third mode corresponds to the noise) in Frappart, Ramillien, Leblanc, et al. (2011). Time series of ICA-based global maps of continental water mass changes from combined UTCSR, JPL and GFZ GRACE solutions, computed over the period 08/2002–12/2010, are used in this study. More details about the post-processing can be found in Frappart et al. (2010), and Frappart, Ramillien, Leblanc, et al. (2011).

2.1.3. GRGS solutions

As for the global Level-2 solutions computed by official providers (CSR, GFZ, and JPL), The Level-2 GRGS-EIGEN-GL04 models are derived from Level-1 GRACE measurements including KBRR, and from LAGEOS-1/2 SLR data for enhancement of lower harmonic degrees (Bruinsma et al., 2010; Lemoine et al., 2007). These gravity fields are expressed in terms of normalized spherical harmonic coefficients of the geopotential (*i.e.*, Stokes coefficients) from degree 2 up to degree 50–60 using an empirical stabilization approach without any smoothing or filtering. This stabilization approach consists in adding empirically-determined degree and order-dependent coefficients to minimize the time variations of the signal measured by GRACE over ocean and desert without significantly affecting the amplitude of the signal over continents. 10-day (Release-2) Total

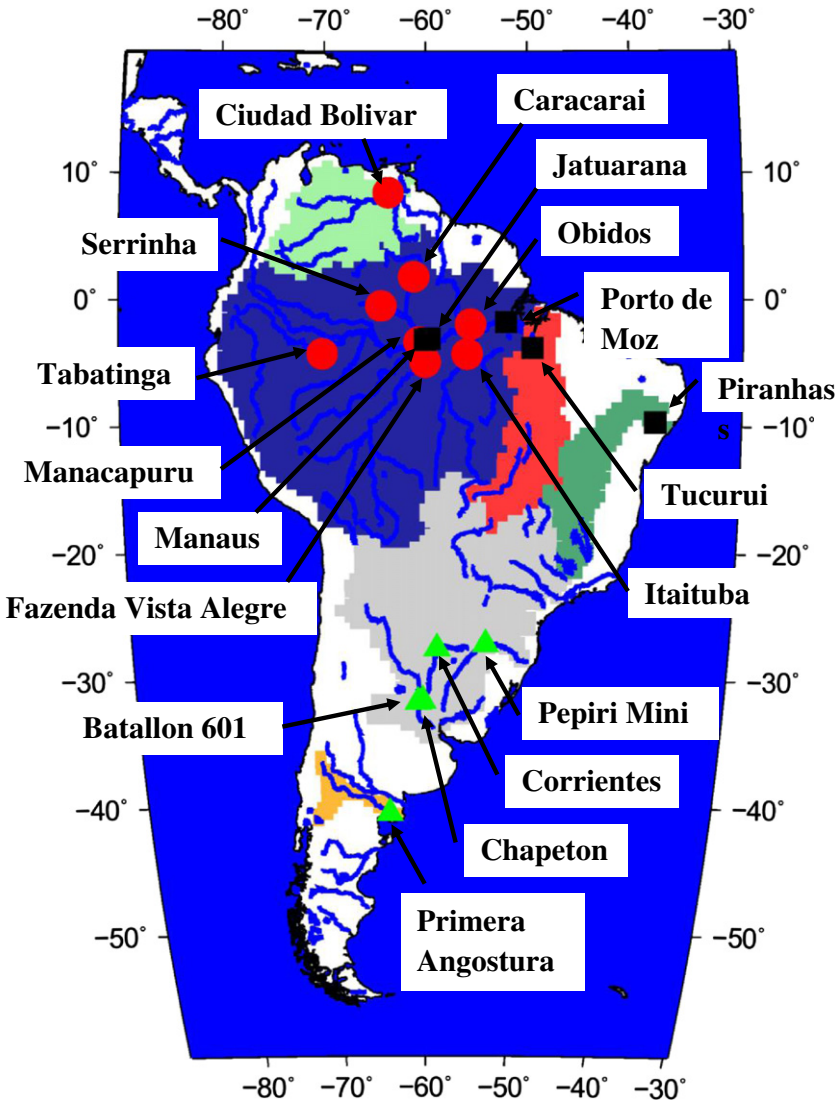

Fig. 1. Major drainage basins of South America: Orinoco (light green), Amazon (dark blue), Tocantins (red), São Francisco (dark green), La Plata (gray), Negro (orange). *In situ* gauge stations are represented with red circles (HYBAM), black squares (ANA), and green triangles (INA).

Table 1
List of the in situ stations used for comparisons with GRACE-derived TWS over the largest river basins South America (Amazon, La Plata, Orinoco, Tocantins, São Francisco, Negro) and their tributaries.

Station	Basin	Lon (°)	Lat (°)	Source
Ciudad Bolivar	Orinoco	−63.608	8.439	HYBAM
Caracarai	Branco (Amazon)	−61.124	1.814	HYBAM
Serrinha	Negro (Amazon)	−64.289	−0.485	HYBAM
Manaus	Negro (Amazon)	−60.035	−3.149	ANA
Tabatinga	Solimões (Amazon)	−69.952	−4.253	HYBAM
Manacapuru	Solimões (Amazon)	−60.609	−3.316	HYBAM
Fazenda Vista Alegre	Madeira (Amazon)	−60.026	−4.898	HYBAM
Jatuarana	Amazon	−59.643	−3.062	ANA
Obidos	Amazon	−55.657	−1.923	HYBAM
Itaituba	Tapajos (Amazon)	−55.982	−4.278	HYBAM
Porto de Moz	Xingu (Amazon)	−52.240	−1.753	ANA
Tucurui	Tocantins	−49.683	−3.783	ANA
Piranhas	São Francisco	−37.756	−9.626	ANA
Corrientes	Parana (La Plata)	−58.833	−27.475	INA
Pepiri Mini	Uruguay (La Plata)	−53.933	−27.154	INA
Batallon 601	Coronda (La Plata)	−60.746	−31.694	INA
Chapeton	Parana (La Plata)	−60.283	−31.574	INA
Primera Angostura	Negro	−63.790	−40.456	INA

Water Storage (TWS) grids of 1-degree spatial resolution available at http://grgs.obs-mip.fr are used over 2003–2010.

2.2. In situ water levels and discharge

Time series of daily water levels from in situ gauges located in the largest drainage basins of South America (Amazon, La Plata, Orinoco, Tocantins, São Francisco, Negro) and their tributaries (Fig. 1 and Table 1) and monthly discharges in Obidos (Amazon), Ciudad Bolivar (Orinoco), Tucurui (Tocantins), and Chapeton (La Plata) were used for

Table 2
Explained variances for the four first modes of the Principal Components Analysis (PCA) of centered and deseasonalized TWS from GRACE for the regional solutions, the ICA-filtered solutions from CSR, GFZ, and JPL, and the GRGS solutions over the 2003–2010 time-period.

Explained variance (%)	Mode 1	Mode 2	Mode 3	Mode 4	Sum
Regional	43	20	13	11	87
ICA CSR	44	15	14	10	83
ICA GFZ	42	17	13	10	82
ICA JPL	41	21	13	8	83
GRGS	60	14	10	8	92

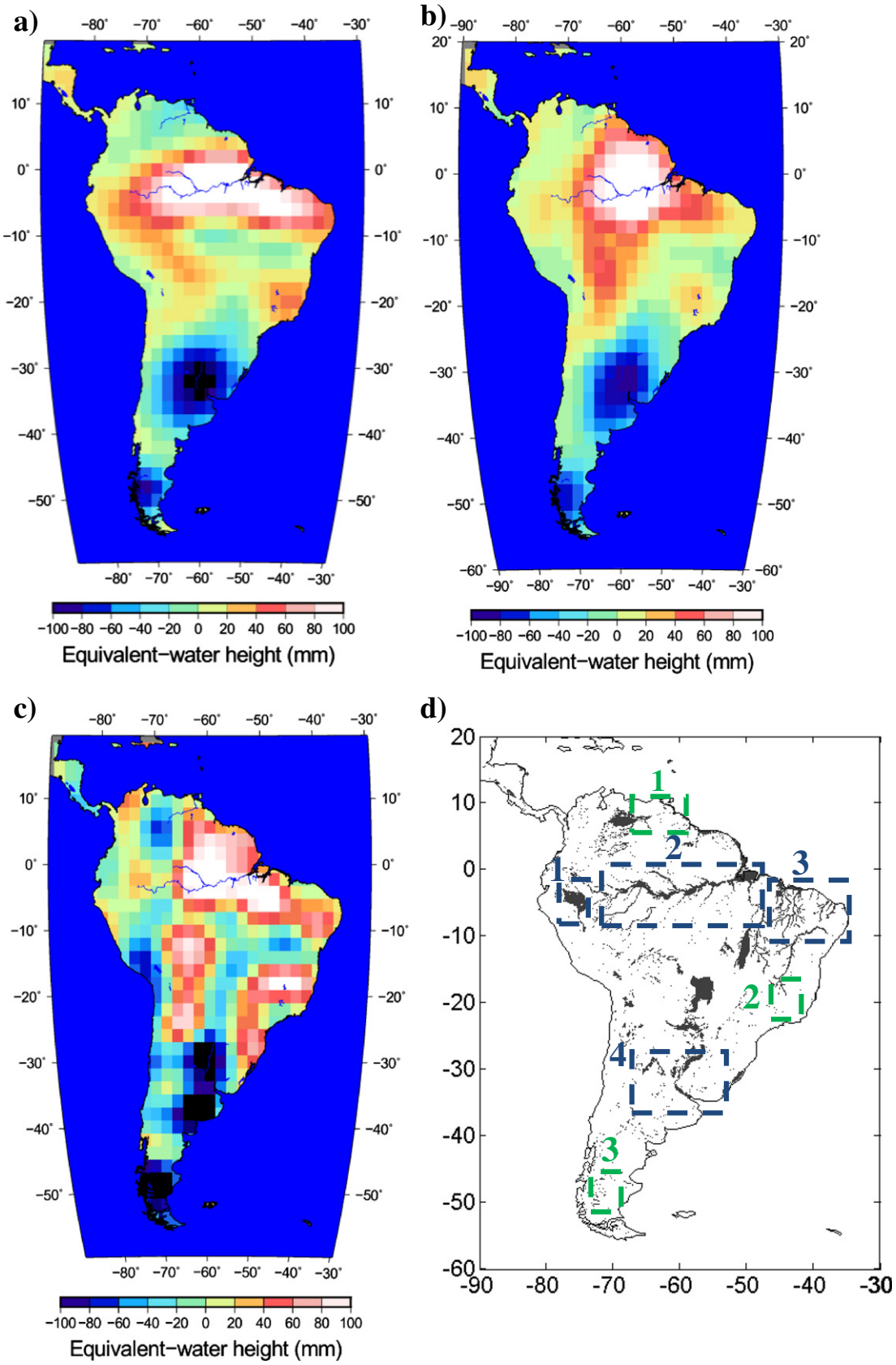

Fig. 2. Spatial component of the 1st PCA mode of TWS for a) Regional ($\sigma^2 = 0.43$), b) ICA-CSR ($\sigma^2 = 0.44$), and c) GRGS ($\sigma^2 = 0.6$) solutions over 2003–2010. d) GLWD map of surface water over South America. In the dashed blue rectangles, regions of maximum or minimum of TWS signal: 1 — Altiplano, 2 — Solimões-Amazon corridor (including the south of the Amazonian Negro basin) + mouth of the Tocantins, 3 — Pindare and Parnacaiba, 4 — La Plata delta. In the dashed green rectangles, secondary extrema of TWS: 1 — Mouth of the Orinoco, 2 — Sources of Parana (La Plata) and São Francisco rivers, 3 — Patagonia Icefield and Deseado basin.

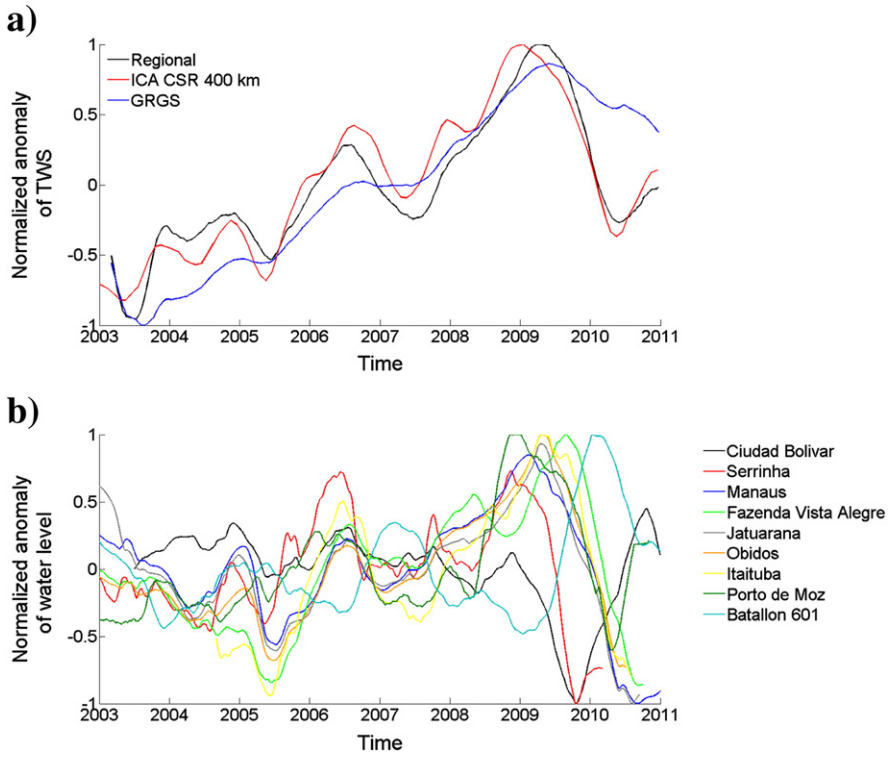

Fig. 3. a) Temporal component of the 1st PCA mode of TWS for Regional (black), ICA-CSR (red), and GRGS (blue) solutions over 2003–2010. b) Time variations of normalized water levels correlated with the 1st PCA mode: Ciudad Bolivar (black), Serrinha (red), Manaus (blue), Fazenda Vista Alegre (light green), Jatuarana (gray), Obidos (orange), Itaituba (yellow), Porto de Moz (dark green), Batallon 601 (light blue).

comparisons to 10-day and monthly anomalies of GRACE-based TWS over 2003–2010. These in situ records were downloaded either from the Environmental Research Observatory (ORE) HYBAM website (http://www.ore-hybam.org/) for the Orinoco basin and some gauges located in the Amazon basin, and from the hydrological information system Hidroweb (http://hidroweb.ana.gov.br/) of the Brazilian water agency (Agência Nacional de Aguas —A NA) for some gauges located in the Amazon and the Tocantins basins, as well as from the Argentinian water agency (Instituto Nacional del Agua — INA) through the online database Base de Datos Hidrológica Integrada (BDHI — http://www.hidricosargentina.gov.ar/) over the period 2002–2011. The seasonal amplitude was removed using a 13-month sliding window on each time-series of daily in situ water levels and monthly discharge.

2.3. Maps of water resources

2.3.1. Floodplains, wetlands and lakes database

The Global Land and Wetlands Database (GLWD) based on the combination of different available cartographic sources is a comprehensive database of global lakes with an area greater than 1 km^2 and provides a good representation of the maximum global wetland extent (Lehner & Döll, 2004). We used the GLWD-3 product with a spatial resolution of 30′ to locate the surface waters (*i.e.*, large-scale wetland distributions and important wetland complexes) over South America.

2.3.2. Groundwater resources map

The Worldwide Hydrological Mapping and Assessment Programme (WHYMAP) made available a 1:25,000,000 map of groundwater resources through the website of the German Federal Institute for Geosciences and Natural Resources (Bundesanstalt für Geowissenschaften un Rohstoffe — BGR): http://www.whymap.org. This map presents the geographical extent of the aquifers and their environmental characteristics: large and rather uniform groundwater basins, complex hydrogeological structures, and limited groundwater resources in local and shallow aquifers (Richts, Struckmeier, & Zaepke, 2011). The groundwater recharge information originates from WGHM model outputs (Döll & Fiedler, 2008).

2.4. Time-series of TWS expressed in terms of equivalent sea level at basin-scale

For a given month t, regional average of TWS expressed in terms of mm of equivalent-water height ($\Delta h_{TWS}(t)$) over a given river basin of area S is computed from the TWS anomaly grid ($\Delta h(\lambda_j,\varphi_j,t)$) at time t of the pixel of longitude and latitude (λ_j,φ_j) with $j = 1, 2, \ldots$ inside S, and the elementary surface $R_e{}^2\ \Delta\lambda\ \Delta\varphi\ cos\ \varphi_j$ (Frappart, Ramillien, & Famiglietti, 2011; Ramillien, Frappart, Cazenave, & Güntner, 2005):

$$\Delta h_{TWS}(t) = \frac{R_e^2}{S}\sum_{j\in S}\Delta h\left(\lambda_j,\phi_j,t\right)\cos\left(\phi_j\right)\Delta\lambda\Delta\phi \tag{1}$$

where R_e is the mean radius of the Earth (6378 km) and $\Delta\lambda$ and $\Delta\varphi$ are the grid steps in longitude and latitude respectively (generally $\Delta\lambda = \Delta\varphi$).

The time-series of TWS expressed in EWH for the four largest South American drainage basins are then converted into Equivalent Sea Level (ESL) ($\Delta h_{TWS\_ESL}(t)$) (Ramillien et al., 2008):

$$\Delta h_{TWS_{ESL}}(t) = \frac{\rho_{SW}S_{basin}}{\rho_{ocean}S_{ocean}}\Delta h_{TWS}(t) \tag{2}$$

where ρ_{SW} and ρ_{ocean} are the densities of soil water and ocean (with the respective values of 1000 and 1030 kg m^{-3}), and S_{basin} and S_{ocean} the surfaces of the considered basin and the global ocean (S_{ocean} = 360 millions of km^2) respectively.

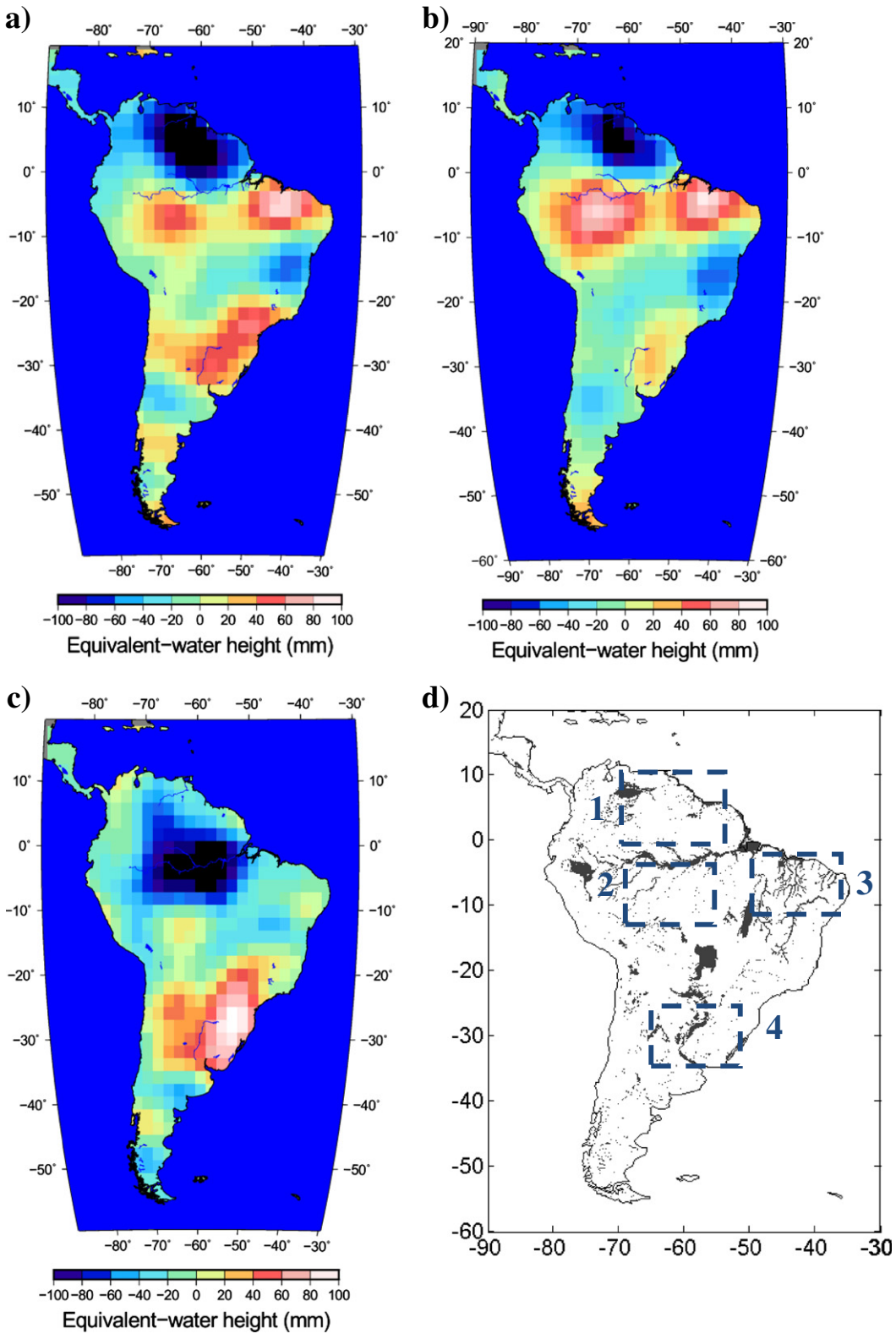

Fig. 4. Spatial component of the 2nd PCA mode of TWS for a) Regional ($\sigma^2 = 0.2$), b) ICA-CSR ($\sigma^2 = 0.15$), and c) GRGS ($\sigma^2 = 0.14$) solutions over 2003–2010. d) GLWD map of surface water over South America. In the dashed blue rectangles, regions of maximum or minimum of TWS signal: 1 — Orinoco and the Negro basins, 2 — the southern bank of the Solimões, 3 — the region covered with Pindare and Parnacaiba basins, 4 — the downstream part and the delta of La Plata basin.

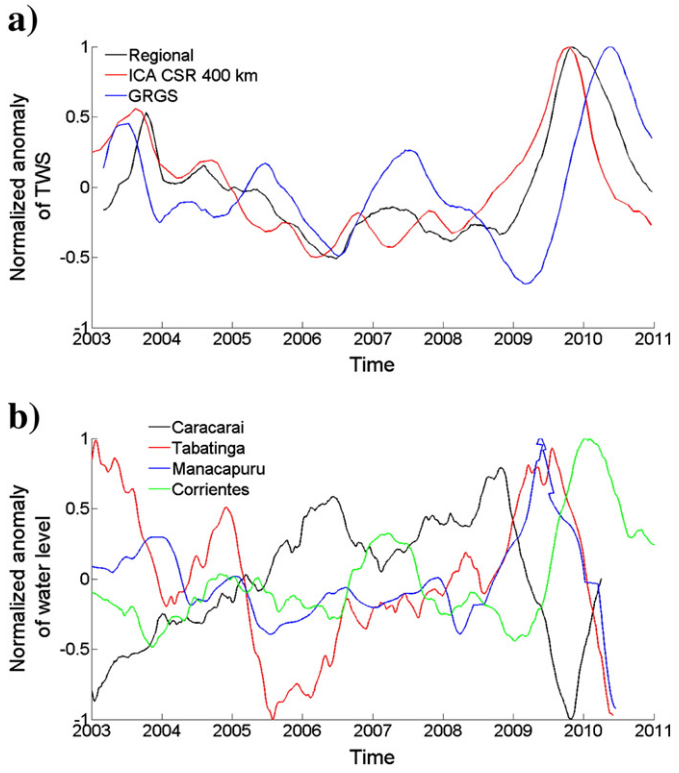

Fig. 5. a) Temporal component of the 2nd PCA mode of TWS for Regional (black), ICA-CSR (red), and GRGS (blue) solutions over 2003–2010. b) Time variations of normalized water levels correlated with the 2nd PCA mode: Caracarai (black), Tabatinga (red), Manacapuru (blue), Corrientes (green).

3. Results

3.1. PCA modes of TWS at interannual time-scale

A Principal Components Analysis (PCA) was applied to the series of GRACE-based TWS from Regional, ICA, and GRGS solutions over South America (−90°–−30°; −60°–20°) for the period 2003–2010, after the removal of the dominant seasonal amplitude using a 13-month sliding window. The sum of the explained variances (σ^2) of the four first PCA modes represents 0.87 for the regional, 0.82 for the ICA-GFZ-400 km (0.83 for both ICA-CSR-400 km and ICA-JPL-400 km), and 0.92 for the GRGS solutions (Table 2). The explained variance by a mode corresponds to the variance in the dataset explained by a PC, the sum of the variances or total variance equals 100%. Most of the seasonally corrected signal present in the GRACE-derived land water solutions is mostly concentrated in these four modes that will be analyzed in detail in the following.

The resulting 4 first modes are respectively presented in Figs. 2, 4, 6, and 8 for the spatial components and in Figs. 3, 5, 7, 9 for the temporal components. Spatial components of the 4 first modes exhibit similar patterns for the different GRACE solutions. Correlations between pairs of GRACE solutions for each spatial mode can be found in Table 3. They are generally higher between regional and ICA solutions than between regional and GRGS solutions (*i.e.*, $R_{(regional;\ ICA)}-R_{(regional;\ GRGS)} > 0.23$), except for the fourth mode. The major difference between the regional and the global solutions is the complete absence in the regional solutions of spurious meridional undulations materialized as north-south stripes, and unfortunately polluting the spatial patterns of the global ones. These north–south stripes appear as one of the major features in the 1st spatial mode of the GRGS solutions (Fig. 2c), and can also be identified in the 2nd spatial mode of the GRGS (Fig. 4c), as well as in the 1st and 4th spatial modes of the ICA solutions (Figs. 2b and 8b respectively) but with a lower intensity. The presence of these stripes accounts for the lower agreement between the 1st mode of GRGS and regional (but also ICA) solutions (Table 3). Besides, for the 2nd and 3rd modes, this lower agreement results from the different geographical locations of the extrema.

The large negative pattern located above the Equator in the 2nd mode of the regional and ICA solutions (Fig. 4a and b respectively) is centered on the Equator in the 2nd mode of the GRGS solutions (Fig. 4c). The two maxima centered around −70° of longitude and −5° of latitude, and −70° of longitude and −5° of latitude (Fig. 4a and b respectively), in the 2nd mode of the regional and ICA solutions, are absent from the 2nd mode of the GRGS solutions (Fig. 4c). Accordingly, the maximum and minimum located on the right and left banks of the Amazon have a different shape in the 3rd mode of the regional and ICA solutions (Fig. 6a and b respectively), and in the 3rd mode of the GRGS solutions (Fig. 6c). This different behavior of the GRGS products compared with other regional and global solutions has already been reported by Klees et al. (2008) over different large continental areas and river basins, and lately by Awange et al. (2011) over Australia. It was attributed to leakage effect (Klees et al., 2008) caused by the low cut-off degree applied to GRGS solutions (*i.e.*, n = 50 or spatial resolution of 400 km) compared to the one applied to other global solutions (*i.e.*, n = 60 for CSR and n = 120 for GFZ and JPL, or spatial resolutions of 333 km and 167 km respectively), and moreover to the north–south striping largely affecting these global solutions (Awange et al., 2011). For the 4th mode, the lower agreement between regional and ICA solutions can be attributed to the smoothness of these solutions that are twice filtered using a Gaussian filter of 400 km of radius before being separated by ICA.

Temporal components of the four 1st modes of the PCA of the GRACE solutions also present quite similar profiles. Cross-correlations between pairs of GRACE solutions for each temporal mode were also computed for time-lag (Δt) varying between ±6 months. Results are presented in Table 4 for $\Delta t = 0$ and Δt maximizing the cross-correlation into the one-year window. Similarly to what was earlier revealed for the spatial components, greater correlations are found between the regional and the ICA solutions than between the regional and the GRGS solutions for smaller time-delays, except for the 4th mode (Table 4). Similar large time-shifts between GRGS and other types of GRACE solutions were already observed over Australia and attributed to the large impact of degrading north–south striping on the restitution of the hydrological signals, especially at interannual time-scales (Awange et al., 2011).

3.2. Relationships between main TWS modes and hydrological features of South America

3.2.1. First mode of variability

South America is covered by large drainage basins where surface waters represent a large part of the TWS measured by GRACE (Frappart, Papa, et al., 2011; Frappart et al., 2008, 2012; Han et al., 2009; Kim, Yeh, Oki, & Kanae, 2009). So, the spatial and temporal components of the PCA of the GRACE-based TWS are respectively compared to the spatial distribution of lakes and reservoirs, rivers and associated floodplains, and wetlands from GLWD (Lehner & Döll, 2004), and the interannual variations of water levels at the mouth of the South America's major rivers and tributaries (see the location of the selected in situ gauges in Fig. 1). We deliberately limited our analysis to the in situ gauges at located at (or close to) the mouth of a (sub-)basin, to be representative of a sufficiently large drainage area, to remain compatible with the spatial resolution of the GRACE-based hydrological products (*i.e.*, 300–400 km).

The spatial component of the PCA first mode is presented in Fig. 2a–c for respectively regional ($\sigma^2 = 0.43$), ICA-CSR-400 km ($\sigma^2 = 0.44$), noted ICA in the followings, and GRGS ($\sigma^2 = 0.6$) land water solutions. In spite of the coarse spatial resolution of the GRACE data, it agrees well with the distribution of surface water

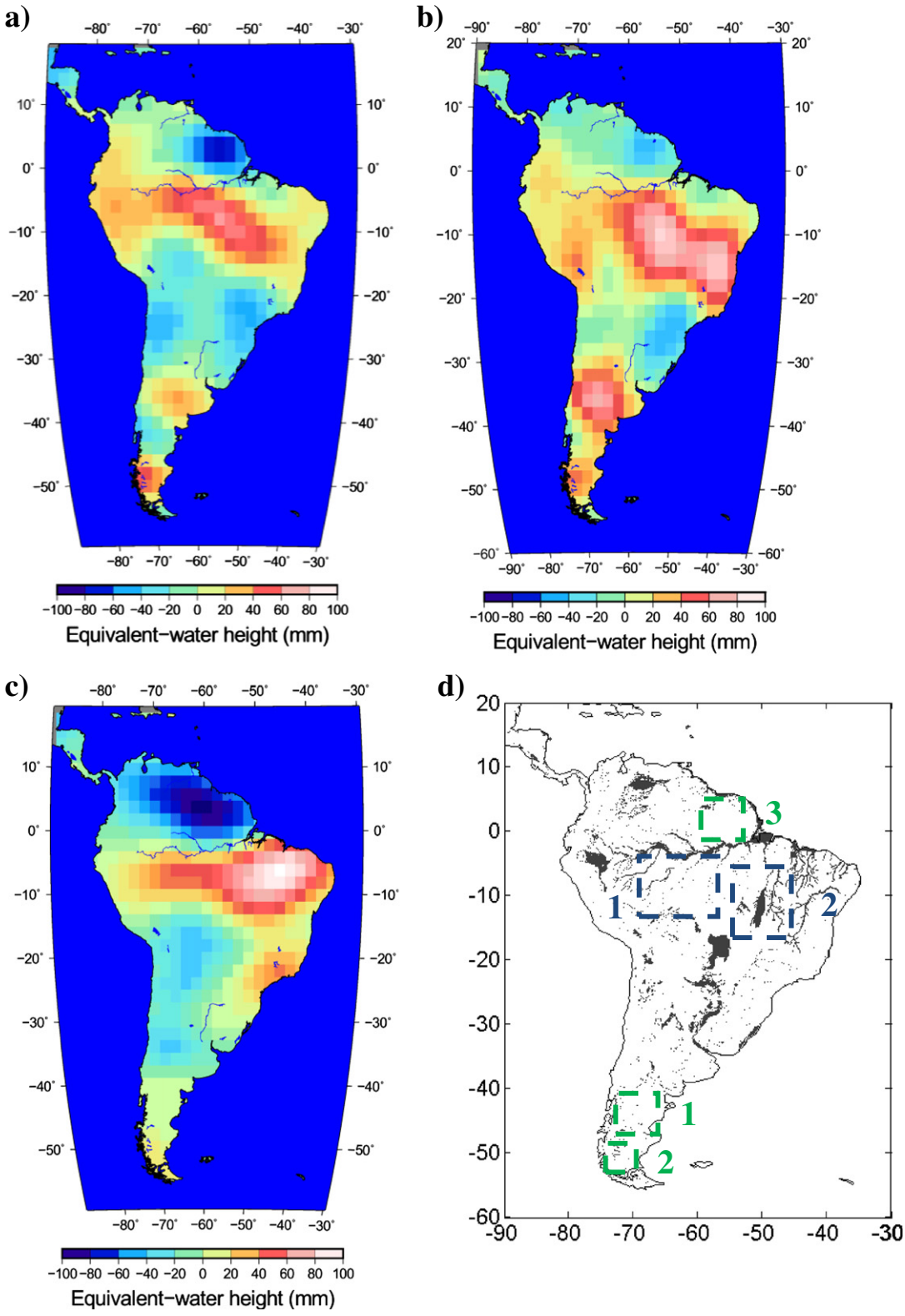

Fig. 6. Spatial component of the 3rd PCA mode of TWS for a) Regional ($\sigma^2 = 0.13$), b) ICA-CSR ($\sigma^2 = 0.14$), and c) GRGS ($\sigma^2 = 0.1$) solutions over 2003–2010. d) GLWD map of surface water over South America. In the dashed blue rectangles, regions of maximum or minimum of TWS signal: 1 — southern bank of the Solimões and the central corridor of the Amazon until the junction with the Tapajos river 2 — upstream part of the Tocantins. In the dashed green rectangles, secondary extrema of TWS: 1 — Negro basin, 2 — Patagonia Icefield and Deseado basin, 3 — Essequibo (Guyana), Suriname (Suriname), Oyapok and Maroni (French Guiana) basins.

from GLWD (Fig. 2d). The strongest amplitudes of the first mode are located in the Altiplano region, area of inland in the Central Andes encompassing Titicaca and Poopó lakes, along the Solimões-Amazon corridor (including the south of the Amazonian and the Negro basins), in the delta of La Plata, upstream the mouth of the Tocantins, and in the region covered with Pindare and Parnacaiba basins

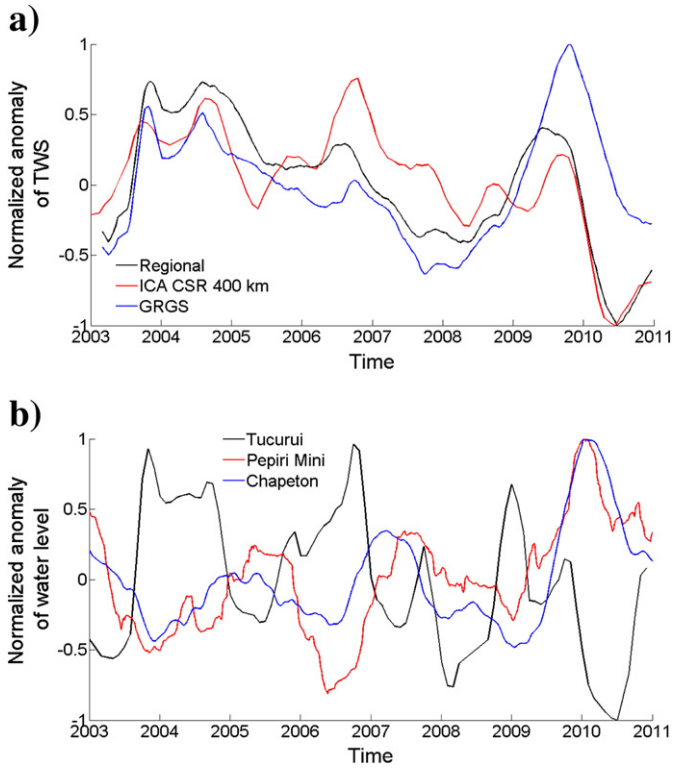

Fig. 7. a) Temporal component of the 3rd PCA mode of TWS for Regional (black), ICA-CSR (red), and GRGS (blue) solutions over 2003–2010. b) Time variations of normalized water levels correlated with the 3rd PCA mode: Tucurui (black), Pepiri Mini (red), Chapeton (blue).

(Fig. 2d). Some secondary extrema are also seen at the mouth of the Orinoco basin, the region of the sources of the Parana (La Plata) and São Francisco rivers, and in the Deseado basin in Patagonia and over Patagonia Icefield (Fig. 2d). These hydrological structures are better concentrated on the regional (Fig. 2a) than on the global spherical harmonics solutions (Fig. 2b and c). One of the main advantages in considering regional solutions is to concentrate the starting GRACE information in a chosen portion of the terrestrial surface (*i.e.*, better spatial localization), instead of dealing with global spectral coefficients (*i.e.*, best frequency localization) (see Freeden & Schreiner, 2008). In the latter case, by construction, the satellite signals are diluted over all the terrestrial sphere, consequently any sharp surface detail should be reconstructed by a quasi-infinite sum of spherical harmonic coefficients, which remains impossible in practice as GRGS and ICA solutions are limited up to degree 50–60. The associated temporal component for each GRACE solutions is presented in Fig. 3a. The three time-series appear very similar, however the GRGS one being smoother. The regional and the ICA solutions exhibit larger negative peaks in 2005 and 2010, and positive in 2009, corresponding to the extreme droughts and flood which strongly affected the Amazon basin (Chen, Wilson, & Tapley, 2010; Chen et al., 2009; Frappart et al., 2012, in press; Marengo, Tomasella, Soares, Alves, & Nobre, 2011; Tomasella et al., 2011), and to the 2009 drought that affected La Plata Basin (Chen et al., 2010; Pereira & Pacino, 2012), than the GRGS solutions. Regional and ICA solutions are almost in phase except for the 2009 extreme flood when the ICA peak is located in the beginning of the year whereas it occurs later (April–May) in the regional solutions, close to the flood peak in the Amazon basin.

Comparisons to in situ gauges highly (anti)correlated to mode 1 are presented in Fig. 3b and Table 5. Please note that anti-correlations come from the arbitrary sign given to both the spatial and temporal components. In all cases, the anti-correlation corresponds to region where the spatial mode has a negative sign.

Mode 1 represents the larger part of the variability observed over South America in the GRACE solutions. It is logically correlated to the largest number of in situ stations used in this study (9 among 18 or 50% with $|R| > 0.65$ for the regional solutions), and to in situ stations (Fig. 1) located in a neighborhood of an extremum or a secondary extremum in the spatial component. Correlations are generally higher for the regional solutions, than for the ICA and GRGS solutions, even if the values are quite high for all type of solutions. High correlation (>0.8) is observed in Obidos located at ~1500 km upstream to the mouth of the Amazon, for all type of solutions with different time-delays between the GRACE solutions and the in situ measurements: −20/30/−120 days between regional/ICA/GRGS solutions and water levels in Obidos respectively (Table 5). The zero time-lag corresponds to the region of maximum of signal located between Jatuarana and Obidos (see Fig. 1), in the center of the downstream Amazon along its mainstem. The opposition of phase between the hydrological signals in the Orinoco and the Amazon basins clearly appears in the time lags for Obidos and Ciudad Bolivar in the regional and ICA solutions. A higher delay is observed upstream in the Madeira tributary at Fazenda Vista Alegre, a much higher one in Manaus, due to the control of the Negro river flow by the Solimões or backwater effect (Meade, Rayol, Conceição, & Navidade, 1991). On the contrary, negative time-lag is found for the Xingu river, in the regional, and mostly, in the ICA solutions (except for Itaituba and Manaus).

This confirms that the Regional solutions are more accurate as they are both spatially and temporally better localized than the global solutions. A large decrease of mass can be identified in the Patagonian Icefield between 2003 and 2009, as a positive trend in the temporal component is multiplied by negative values in the spatial component. This confirms what was already observed by Chen, Wilson, Tapley, Blankenship, and Ivins (2007) using GRACE data.

3.2.2. Second mode of variability

The spatial components of the second mode of PCA are presented in Fig. 4a–c for Regional ($\sigma^2 = 0.2$), ICA ($\sigma^2 = 0.15$), and GRGS ($\sigma^2 = 0.14$) land water solutions, respectively. The extrema present in the Regional (Fig. 4a) and ICA (Fig. 4b) are centered on the Orinoco and the Negro basins (*i.e.*, negative patterns in the northern part of South America), the southern bank of the Solimões, the region covered with both Pindare and Parnacaiba basins, and the downstream part and the delta of La Plata basin (positive patterns in the western, eastern, and south eastern parts of the continent respectively). These structures are in good agreement with the distribution of surface water from GLWD (Fig. 4d). The spatial patterns of the 2nd mode of PCA for the GRGS are quite different, as a large negative pattern appears on the central corridor of the Amazon, at the junction between the Solimões, Negro and Madeira rivers, and no positive pattern over the southern bank of the Solimões, and neither in the region covered with Pindare and Parnacaiba basins.

Four in situ stations (~20%) were found to have high correlations with the 2nd mode temporal mode of the PCA of the GRACE-derived TWS (Table 5). Three of them are located in the Amazon basin: one in the Branco basin, sub-basin of the Negro basin, northern Amazon where high correlations are obtained ($|R| > 0.8$), especially for the regional and the ICA solutions, and two in the Solimões basin, at its entrance (Tabatinga) and its mouth (Manacapuru). For these two latter stations, high correlations are found between in situ water levels and GRACE-based TWS from regional and ICA solutions, but not from GRGS ($R < 0.5$) (Table 5). The last one is located in La Plata basin and better agreement is found between these water level records and GRGS-derived solutions than regional-derived and ICA-derived solutions. This appears clearly on Fig. 5 presenting the temporal component of the 2nd PCA mode for each set of GRACE solutions (Fig. 5a) and the time-series of in situ water levels for these 4 four stations (Fig. 5b).

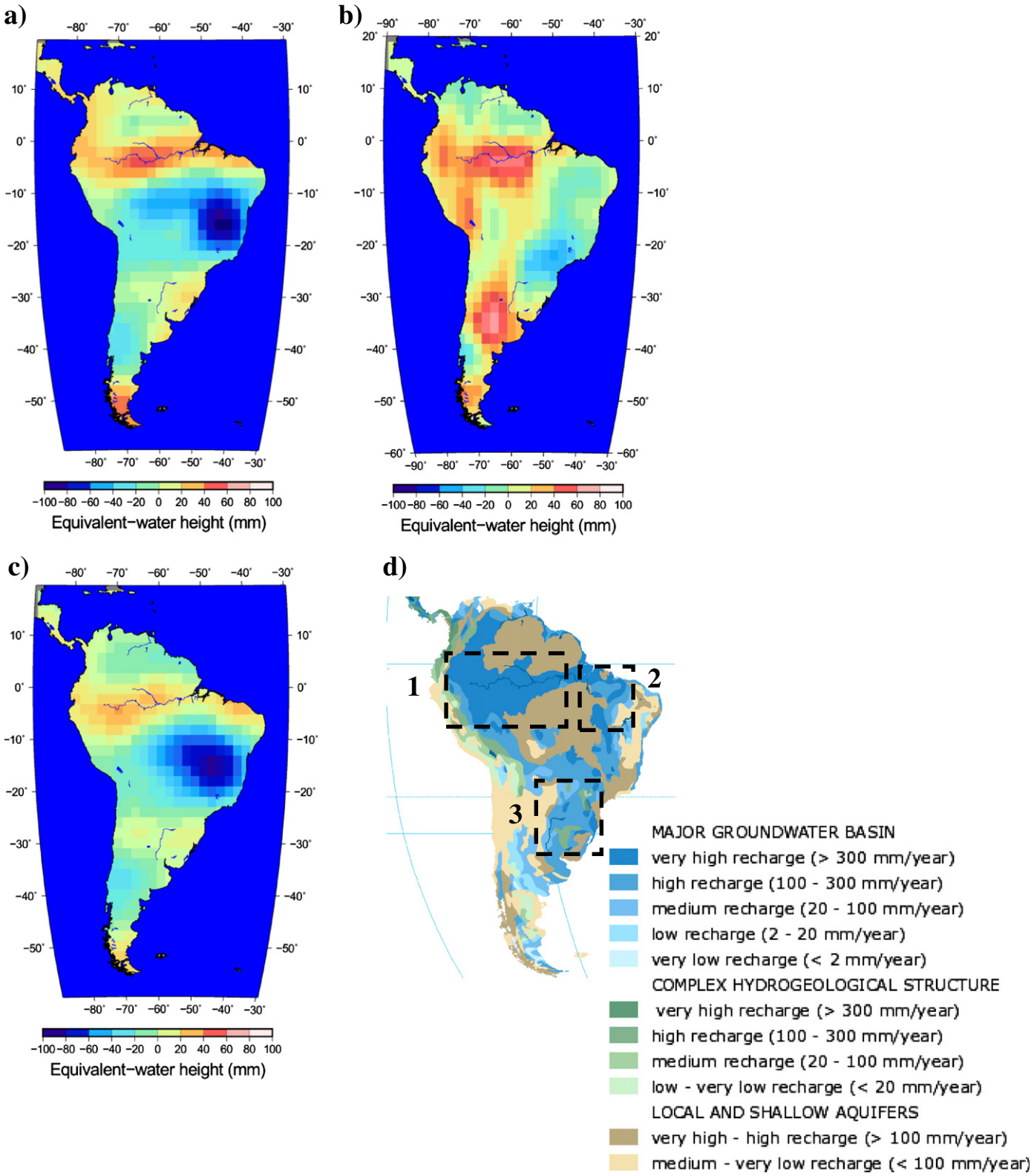

Fig. 8. Spatial component of the 4th PCA mode of TWS for a) Regional ($\sigma^2 = 0.11$), b) ICA-CSR ($\sigma^2 = 0.1$), and c) GRGS ($\sigma^2 = 0.08$) solutions over 2003–2010. d) WHYMAP map of groundwater recharge over South America. In the dashed black rectangles, regions of maximum or minimum of TWS signal: 1 — Amazonas, 2 — Maranhão, 3 — Guarani aquifer systems. These rectangles include the boundaries of the major aquifer systems of South America as presented in Margat (2007).

A time lag of nine months clearly separate the maxima of regional and ICA solutions (*i.e.*, northern hemisphere summer 2009) to the maximum of GRGS solutions (*i.e.*, northern hemisphere winter 2010). They respectively correspond to the extreme flood that affected the Amazon basin in 2009 (Marengo et al., 2011) and to a flooding event occurring in La Plata basin from December 2009 to April 2010 (Salvia et al., 2011).

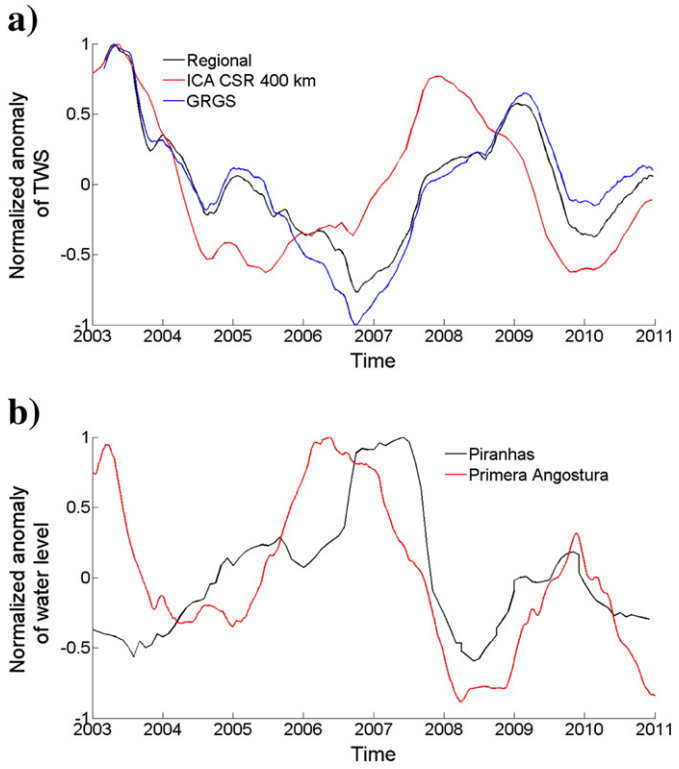

Fig. 9. a) Temporal component of the 4th PCA mode of TWS for Regional (black), ICA-CSR (red), and GRGS (blue) solutions over 2003–2010. b) Time variations of normalized water levels correlated with the 4th PCA mode: Piranhas (black), Primera Angostura (red).

3.2.3. Third mode of variability

The spatial component of the third PCA mode is presented in Fig. 6a–c for regional ($\sigma^2 = 0.13$), ICA ($\sigma^2 = 0.14$), and GRGS ($\sigma^2 = 0.1$) land water solutions respectively (Table 2). As for mode 2, a better agreement is found between regional and ICA solutions than between regional and GRGS solutions, with correlation coefficients equal to 0.69 and 0.46 respectively (Table 3). The maxima in the regional (Fig. 6a) and ICA (Fig. 6b) are located in the southern bank of the Solimões and the central corridor of the Amazon river up to its junction with the Tapajos river, and the upstream part of the Tocantins basin. Once again, this structure is in good agreement with the distribution of surface water from GLWD (Fig. 6d). Some secondary extrema can also be observed in the Negro basin in Argentina, over the Patagonia Icefield and Deseado basin in Patagonia in the south. In the north, extrema are centered over the Essequibo (Guyana), Suriname (Suriname), Oyapok and Maroni (French Guiana) basins (negative). GRGS solutions show that the extrema are located around the central corridor of the Amazon river: negative in the north (northern tributaries and Orinoco). Positive extrema appear in the south and over the Tocantins, Pindare, and Parnacaiba basins for the GRGS solutions.

Its temporal component was found to be correlated ($|R| > 0.7$) to the time-variations of three in situ stations (~15%) located in the Tocantins (Tucurui) and the eastern and southern parts of La Plata (Chapeton and Pepiri Mini), for the regional and ICA solutions. However, the temporal mode for the GRGS solutions is not correlated to in situ records (Table 5).

3.2.4. Fourth mode of variability

The spatial component of the fourth PCA mode is presented in Fig. 8a–c for regional ($\sigma^2 = 0.11$), ICA ($\sigma^2 = 0.1$), and GRGS ($\sigma^2 = 0.08$) land water solutions respectively (Table 2). Correlation is much higher between regional and GRGS solutions (R = 0.86) than between regional and ICA solutions (R = 0.46) (Table 3). North–south stripes clearly appear for the ICA solutions (Fig. 8b). Patterns of TWS seem to be related to the spatial distribution of groundwater recharge from WHYMAP (Fig. 8d). Positive and negative extrema of TWS are located over regions where recharge is maximum: the central corridor of the Amazon river, the downstream part of the Tocantins, the Pindare and the Parnacaiba, and the eastern part of La Plata basin (Fig. 8d). They correspond to the locations of the largest aquifers of South America: Amazonas and Maranhão basins, Guarani Aquifer

Table 3
Correlation between the spatial component of the different GRACE solutions (regional, ICA-CSR-400 km, and GRGS) for each PCA mode.

R	GRACE solutions		
PCA mode	Regional *vs.* ICA-CSR-400 km	Regional *vs.* GRGS	ICA-CSR-400 km *vs.* GRGS
Mode 1	0.84	0.6	0.67
Mode 2	0.67	0.43	−0.04
Mode 3	0.69	0.46	0.38
Mode 4	0.46	0.86	0.39

Table 4
Correlation between the temporal component of the different GRACE solutions (regional, ICA-CSR-400 km, and GRGS), and maximum correlation and associated time-lag for each PCA mode.

R		GRACE solutions		
PCA mode		Regional *vs.* ICA-CSR-400 km	Regional *vs.* GRGS	ICA-CSR-400 km *vs.* GRGS
Mode 1	R(Δt = 0)	0.95	0.82	0.81
	Rmax (Δt in days)	0.96 (30)	0.84 (80)	0.86 (180)
Mode 2	R(Δt = 0)	0.79	0.52	0.08
	Rmax (Δt in days)	0.91 (−120)	0.80 (−160)	0.58 (−180)
Mode 3	R(Δt = 0)	0.79	0.56	0.17
	Rmax (Δt in days)	0.79 (0)	0.61 (−60)	0.21 (60)
Mode 4	R(Δt = 0)	0.62	0.96	0.47
	Rmax (Δt in days)	0.7 (−120)	0.96 (0)	0.57 (180)

Table 5
Correlation value corresponding to maximum of module of correlation and associated time-lag (days) between interannual variations of in situ water levels and GRACE-based TWS for regional, ICA (CSR), and GRGS solutions.

Station	PCA mode	Regional		ICA		GRGS	
		R max(|R|)	Δt (days)	R max(|R|)	Δt (days)	R max(|R|)	Δt (days)
Ciudad Bolivar	1	−0.80	180	−0.73	180	−0.63	170
Caracarai	2	−0.86	−40	−0.83	30	−0.66	−120
Serrinha	1	0.66	−160	0.62	−150	0.62	−180
Manaus	1	0.65	120	0.65	60	0.50	−180
Tabatinga	2	0.81	−160	0.83	−90	0.39	−180
Manacapuru	2	0.91	−180	0.83	−90	0.47	−180
Fazenda Vista Alegre	1	0.80	50	0.84	90	0.75	−160
Jatuarana	1	0.70	30	0.70	60	0.58	−180
Obidos	1	0.88	−20	0.87	30	0.81	−120
Itaituba	1	0.96	0	0.83	−110	0.94	30
Porto de Moz	1	0.88	−90	0.82	0	0.71	−160
Tucurui	3	0.74	−30	0.73	30	0.31	−30
Piranhas	4	0.68	−30	0.71	−30	0.71	−30
Pepiri Mini	3	−0.70	−150	−0.80	−120	−0.16	−180
Corrientes	2	0.71	70	0.52	60	0.90	−100
Batallón 601	1	−0.67	−110	−0.62	−90	0.25	180
Chapeton	3	−0.77	−160	−0.72	−150	−0.39	−180
Primera Angostura	4	−0.70	−150	−0.52	180	−0.77	−150

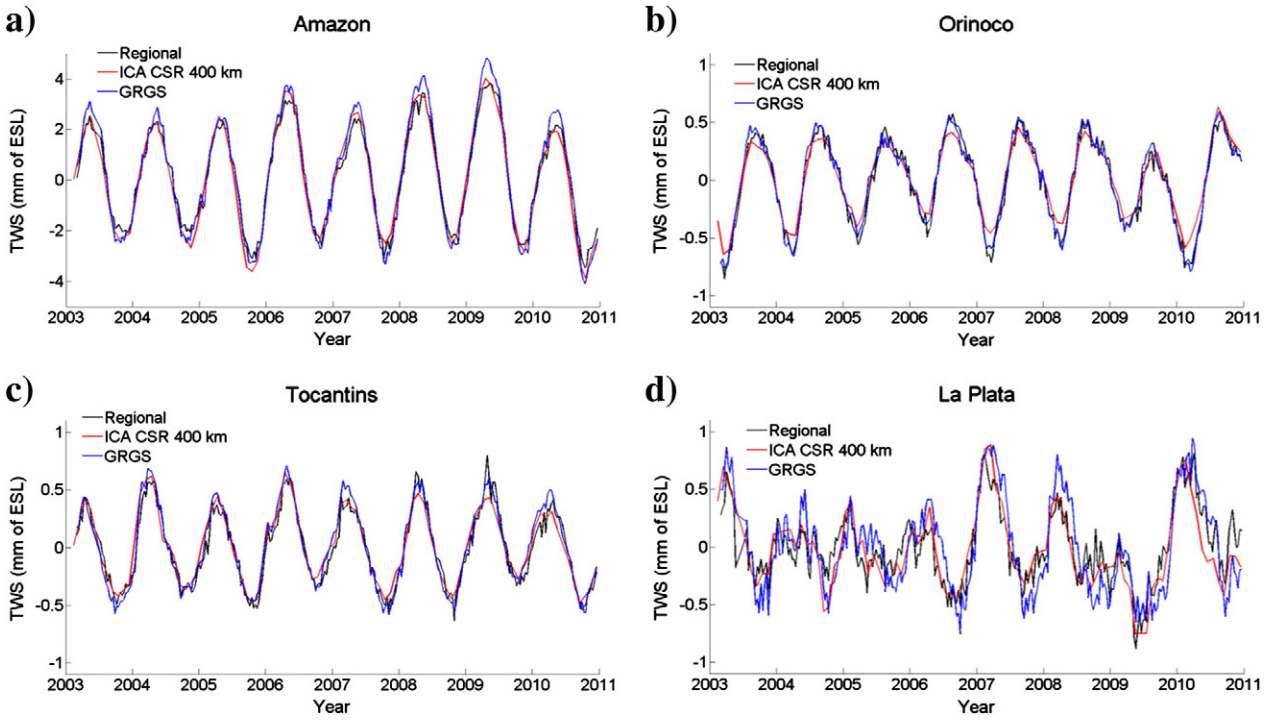

Fig. 10. Time-series of GRACE-based TWS over 2003–2010 from Regional (black), ICA CSR 400 km (red), GRGS (blue) expressed in mm of ESL for the a) Amazon, b) Orinoco, c) Tocantins, and d) La Plata basins.

System respectively (Margat, 2007), and to a region of high to very high recharge according to WHYMAP, located between the two latter basins, which makes part of the groundwater footprint (*i.e.*, the area required to sustain groundwater use and groundwater-dependent ecosystem services of a region of interest, such as an aquifer, watershed or community) of the Maranhão according to Gleeson, Wada, Bierkens, and van Beek (2012) (see Fig. 1 of this paper). The temporal component of the fourth mode is highly correlated to the time-series of water levels of

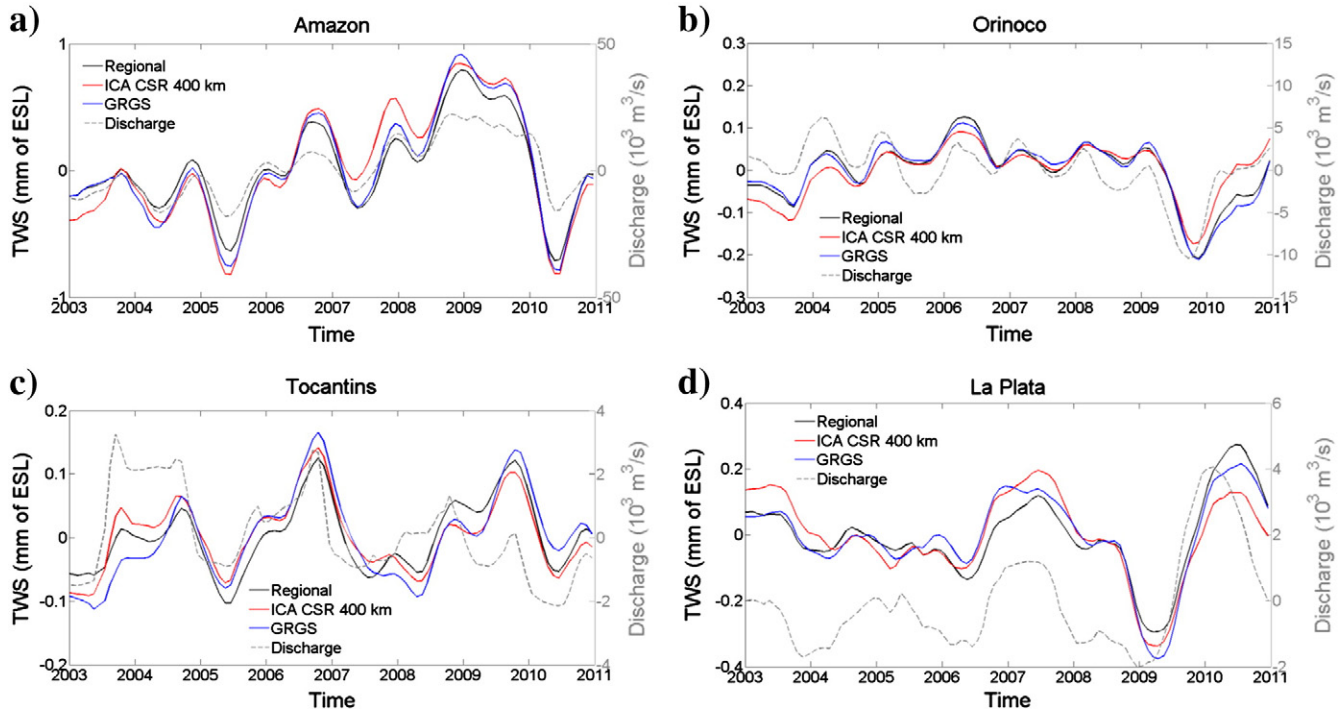

Fig. 11. Time-series of GRACE-based interannual TWS over 2003–2010 from Regional (black), ICA CSR 400 km (red), GRGS (blue) expressed in mm of ESL and of interannual discharge (gray) for the a) Amazon, b) Orinoco, c) Tocantins, and d) La Plata basins.

Table 6
Maximum correlation and associated time-lag (months) between interannual variations of GRACE-based TWS (expressed in ESL) for regional, ICA (CSR), and GRGS solutions of in situ river discharge in Obidos–Amazon, Ciudad Bolivar–Orinoco, Tucurui–Tocantins, and Chapeton–La Plata.

Discharge station	TWS regional		TWS ICA		TWS GRGS	
	Rmax	Δt (months)	Rmax	Δt (months)	Rmax	Δt (months)
Obidos (Amazon)	0.9	1	0.93	1	0.92	1
Ciudad Bolivar (Orinoco)	0.69	−1	0.58	−1	0.69	−2
Tucurui (Tocantins)	0.46	2	0.63	1	0.37	2
Chapeton (La Plata)	0.86	−3	0.61	−3	0.75	−3

two in situ stations (~10%) located in the São Francisco and the Negro (in Argentina) basins.

3.3. Contribution to the major South American drainage basins to sea level

3.3.1. Time series of equivalent sea level in large drainage basins

By dividing the water volume variations by the total ocean surface (~360 millions of km^2), the Equivalent Sea Level (ESL) time series are simply obtained (Fig. 10). They correspond to the water mass contributions of these drainage basins to the actual measured sea level. The ESL time series of regional, GRGS and ICA-400 km solutions remain very close to each other. However, GRGS-based solutions present slightly greater amplitudes when they are averaged over the South American basins. In general, the ESL time series are dominated by a strong seasonal cycle, as previous shown by Ramillien et al. (2008) while using 3-year GRACE data, that reaches ±2 mm for the Amazon river basin. This latter river basin appears as the largest contributor of water mass to the oceans at annual time scale, while the three others have amplitudes of ±0.5 mm ESL. Besides, these series exhibit clear multi-year variations and modulations of the dominant seasonal cycle: in the case of the Amazon, the maxima are important (up to 4 mm ESL) in 2006, 2008 and 2009 only, whereas the curve for La Plata basin contains short wavelengths with maxima of seasonal cycle in 2003, 2007 and 2010. As both time-series of 10-day solutions (*i.e.*, regional and GRGS) exhibit important "high-frequency" variations, their origin seems to be related to sub-monthly hydrological events. Analysis of daily water levels over 37 years (1961–1997) at Corrientes, the closest station to the mouth of La Plata basin, shows larger standard deviations for a lower annual cycle than a similar analysis performed in Obidos (over 27 years), the closest station to the mouth of La Plata basin (Clarke, Mendiondo, & Brusa, 2000). This suggests important short-term hydrological variations in the surface reservoir that can account for the rapid variations observed in Fig. 10d.

3.3.2. Interannual variations of TWS and discharges in large drainage basins

The contribution to sea level variations at interannual time-scale of the largest drainage basins of South America (*i.e.*, Amazon, Orinoco, and Tocantins) is presented on Fig. 11. If the 12-month cycle is removed by applying a 13-month average sliding window on each ESL time-series, it is clear the inter-annual residuals will not be explained by a simple linear trend for the considered 2003–2010 period (Fig. 11). The signatures of the extreme and sudden climatic events that recently affected the Amazon basin as the droughts of 2005 and 2010 and the flood of 2009 (Fig. 11a), and La Plata such as the drought of 2009 and the flood of 2010 (Fig. 11d) can be clearly identified. This is in contradiction with the self-made idea that continents would provide (or retain) water mass to the oceans continuously, by suggesting that multi-year variations do not permit to establish a definitive water mass balance. Moreover, errors in the determination of the long-term mass balance remain comparable to the fitted linear trend values themselves (~0.03 mm/yr), according to Ramillien et al. (2008). In the case of spherical harmonics representation (*i.e.*, GRGS and ICA solutions), most of uncertainty (up to 0.05 mm ESL) is due to spectral leakage (*i.e.*, pollution of signals from other parts of the globe) because of truncation at degree 50–60 (Frappart, Ramillien, Leblanc, et al., 2011). This motivates us to compare the inter-annual variations to independent datasets such as discharge change measurements *versus* time, to confirm the quality of our water mass estimates computed from the different GRACE datasets. The interannual variations of TWS are compared to the interannual variations of river discharges for these large drainage basins of South America. They exhibit similar patterns as already observed in the Amazon basin and its sub-basins using the ICA solutions (Frappart et al., 2012, in press). High correlations ($R \geq 0.9$) were found in the Amazon basin with one month of delay between TWS and discharge (Table 6). This delay can be accounted for the presence of extensive floodplains along the central corridor of the Amazon-Solimões, and over Negro (northern tributary of the Amazon) and Mamoré basins, that cover more than 300,000 km^2 of the surface of the basin (Diegues, 1994; Junk, 1997). The presence of floodplains delays the transit of surface water. As a consequence, TWS is dominated by surface water causing a time-shift between TWS and discharge. On the contrary, for basins less densely covered with floodplains as the Orinoco and La Plata, correlation in time between TWS and discharge remains high ($R \sim 0.7$ except for the ICA solutions with $R \sim 0.6$ and $R > 0.75$ except for the ICA solutions with $R \sim 0.6$ respectively), however the time shift is negative: maximum of discharge occurs one or two months before the maximum of TWS (Table 6). In the Tocantins basin, correlation between TWS and discharge is much lower ($R < 0.6$) most likely because the interannual variations of TWS are more influenced by the groundwater storage, as the region is characterized by the presence of a large aquifer system (Maranhão basin).

4. Conclusion

2-by-2 degree regional water mass solutions over South America were compared to GRACE-based global products (GRGS and ICA-400) for the period 2003–2010, and it is shown that they offer a better geographical location of hydrological structures by construction than global solutions. As a consequence, the higher power spectral density present in the regional solution at smaller spatial scales can be attributed to a better determination of these wavelengths in the regional solutions. Besides, the global GRGS solutions suffer from the presence of residuals North–South striping from aliasing, this effect masks the hydrological structures, and consequently degrades the water mass balance estimates. Principal Component Decomposition of all the GRACE datasets permitted us to unravel modes of variability from observed signals observed by GRACE, and then identify geographical locations of interannual water mass variations of individual groundwater unit over the continent, and correlate them to climatology. Robust validation of these GRACE datasets consists of comparing them to time variations of in situ water level and discharge measurements. Correlations between GRACE solutions and river level records are significant for the four first PCA modes suggesting that these modes represent water mass changes at the surface of the Earth. In particular, signature of the melt of the Patagonian IceField in the gravity field is found in temporal modes 1 and 3 while its location is well identified in the corresponding spatial modes. Temporal mode number 4 seems to be mostly related to slower groundwater variations, as the corresponding spatial mode clearly coincides with the geographical limits of groundwater unit. High correlations are also found between TWS and river discharges at interannual time-scale in the Amazon and Orinoco basins where TWS is dominated by the surface reservoir due to the presence of extensive floodplains, whereas low correlation is found for the Tocantins, likely

because the measured gravity signal is dominated by groundwater changes in this basin. Our study, based on the use of PCA, demonstrated the ability of GRACE satellite gravimetry to distinguish efficiently real hydrological signals in different reservoirs (surface waters, groundwater, glaciers) especially through such a regional approach.

Acknowledgments

The authors would like to thank Dr. Wilhelm Struckmeier and Dipl.-Geogr. Andrea Richts from BGR for letting us use the WHYMAP map of groundwater resources in our paper and to Daniel Cielak, Administrador Banco de Datos Hidrológico, Subsecretaría de Recursos Hídricos de la Nación, Argentina, for giving us acces to the discharges at Chapeton.

References

Alsdorf, D. E., & Lettenmaier, D. P. (2003). Tracking fresh water from space. *Science*, *301*, 1492–1494.

Andersen, O. B., Seneviratne, S. I., Hinderer, J., & Viterbo, P. (2005). GRACE-derived terrestrial water storage depletion associated with the 2003 European heat wave. *Geophysical Research Letters*, *32*(18), L18405.

Awange, J. L., Fleming, K. M., Kuhn, M., Featherstone, W. E., Heck, B., & Anjasmara, I. (2011). On the suitability of the 4° × 4° GRACE mascon solutions for remote sensing Australian hydrology. *Remote Sensing of Environment*, *115*(3), 864–875.

Bergmann, I., Ramillien, G., & Frappart, F. (2012). Climate-driven interannual variations of the mass balance of Greenland. *Global and Planetary Change*, *82–83*, 1–11. http://dx.doi.org/10.1016/j.gloplacha.2011.

Bruinsma, S., Lemoine, J. -M., Biancale, R., & Valès, N. (2010). CNES/GRGS 10-day gravity models (release 2) and their evaluation. *Advances in Space Research*, *45*(4), 587–601. http://dx.doi.org/10.1016/j.asr.2009.10.012.

Chen, J. L., Wilson, C. R., & Tapley, B. D. (2010). The 2009 exceptional Amazon flood and interannual terrestrial water storage change observed by GRACE. *Water Resources Research*, *46*(12), W12526. http://dx.doi.org/10.1029/2010WR009383.

Chen, J. L., Wilson, C. R., Tapley, B. D., Blankenship, D. D., & Ivins, E. R. (2007). Patagonia Icefield melting observed by Gravity Recovery and Climate Experiment (GRACE). *Geophysical Research Letters*, *34*(22), L22501.

Chen, J. L., Wilson, C. R., Tapley, B. D., Longuevergne, L., Yang, Z. L., & Scanlon, B. R. (2010). Recent La Plata basin drought conditions observed by satellite gravimetry. *Journal of Geophysical Research*, *115*, D22108. http://dx.doi.org/10.1029/2010JD014689.

Chen, J. L., Wilson, C. R., Tapley, B. D., Yang, Z. L., & Niu, G. Y. (2009). 2005 drought event in the Amazon River basin as measured by GRACE and estimated by climate models. *Journal of Geophysical Research*, *114*, B05404. http://dx.doi.org/10.1029/2008JB006056.

Clarke, R. T., Mendiondo, E. M., & Brusa, L. C. (2000). Uncertainties in mean discharges from two large South American rivers due to rating curve variability. *Hydrological Sciences Journal-Journal Des Sciences Hydrologiques*, *45*(2), 221–236.

Diegues, A. C. S. (Ed.). (1994). *An inventory of Brazilian wetlands*. Gland, Switzerland: International Union for Conservation of Nature (224 pp.).

Döll, P., & Fiedler, K. (2008). Global-scale modeling of groundwater recharge. *Hydrology and Earth System Sciences*, *12*, 863–885. http://dx.doi.org/10.5194/hess-12-863-2008.

Eicker, A. (2008). *Gravity field refinement by radial basis functions from in-situ satellite data.* (Dissertation). Univ. Bonn D 98. Bonn, Germany: Univ. Bonn, 137.

Frappart, F., Papa, F., Famiglietti, J. S., Prigent, C., Rossow, W. B., & Seyler, F. (2008). Interannual variations of river water storage from a multiple satellite approach: a case study for the Rio Negro River basin. *Journal of Geophysical Research*, *113*(D21), D21104. http://dx.doi.org/10.1029/2007JD009438.

Frappart, F., Papa, F., Güntner, A., Werth, S., Santos da Silva, J., Seyler, F., Prigent, C., Rossow, W. B., Calmant, S., & Bonnet, M. -P. (2011). Satellite-based estimates of groundwater storage variations in large drainage basins with extensive floodplains. *Remote Sensing of Environment*, *115*(6), 1588–1594. http://dx.doi.org/10.1016/j.rse.2011.02.003.

Frappart, F., Papa, F., Santos da Silva, J., Ramillien, G., Prigent, C., Seyler, F., et al. (2012). Surface freshwater storage in the Amazon basin during the 2005 exceptional drought. *Environmental Research Letters*, *7*(4), 044010. http://dx.doi.org/10.1088/1748-9326/7/044010.

Frappart, F., Ramillien, G., & Famiglietti, J. S. (2011). Water balance of the Arctic drainage system using GRACE gravimetry products. *International Journal of Remote Sensing*, *32*(2), 431–453. http://dx.doi.org/10.1080/01431160903474954.

Frappart, F., Ramillien, G., Leblanc, M., Tweed, S. O., Bonnet, M. -P., & Maisongrande, P. (2011). An independent component analysis approach for filtering continental hydrology in the GRACE gravity data. *Remote Sensing of Environment*, *115*(1), 187–204. http://dx.doi.org/10.1016/j.rse.2010.08.017.

Frappart, F., Ramillien, G., Maisongrande, P., & Bonnet, M. -P. (2010). Denoising satellite gravity signals by independent component analysis. *IEEE Geoscience and Remote Sensing Letters*, *7*(3), 421–425. http://dx.doi.org/10.1109/LGRS.2009.2037837.

Frappart, F., Ramillien, G., & Ronchail, J. (2013). Changes in terrestrial water storage vs. rainfall and discharges in the Amazon basin. *International Journal of Climatology*. http://dx.doi.org/10.1002/joc.3647 (in press).

Freeden, W., & Schreiner, M. (2008). *Spherical functions of mathematical geosciences: A scalar, vectorial, and tensorial setup.* Heidelberg: Springer (602 pp.).

Gleeson, T., Wada, Y., Bierkens, M. F. P., & van Beek, L. P. H. (2012). Water balance of global aquifers revealed by groundwater footprint. *Nature*, *488*, 197–200. http://dx.doi.org/10.1038/nature11295.

Han, S. -C., Kim, H., Yeo, I. Y., Yeh, P., Oki, T., Seo, K. W., et al. (2009). Dynamics of surface water storage in the Amazon inferred from measurements of inter-satellite distance change. *Geophysical Research Letters*, *36*, L09403. http://dx.doi.org/10.1029/2009GL037910.

Junk, W. J. (1997). General aspects of floodplain ecology with special reference to Amazonian floodplains. In W. J. Junk, M. T. F. Piedade, F. Wittmann, J. Schöngart, & P. Parolin (Eds.), *The central Amazon floodplain: Ecology of a pulsing system* (pp. 3–20). Berin & Heidelberg, Germany: Springer-Verlag.

Kim, H., Yeh, P. J. F., Oki, T., & Kanae, S. (2009). Role of rivers in the seasonal variations of terrestrial water storage over global basins. *Geophysical Research Letters*, *36*, L17402. http://dx.doi.org/10.1029/2009GL039006.

Klees, R., Liu, X., Wittwer, T., Gunter, B. C., Revtova, E. A., Tenzer, R., et al. (2008). A comparison of global and regional GRACE models for land hydrology. *Surveys in Geophysics*, *29*(4–5), 335–359.

Leblanc, M. J., Tregoning, P., Ramillien, G., Tweed, S. O., & Fakes, A. (2009). Basin-scale, integrated observations of the early 21st century multiyear drought in southeast Australia. *Water Resources Research*, *45*, W04408. http://dx.doi.org/10.1029/2008WR007333.

Lehner, B., & Döll, P. (2004). Development and validation of a global database of lakes, reservoirs and wetlands. *Journal of Hydrology*, *296*(1–4), 1–22.

Lemoine, J. -M., Bruinsma, S., Loyer, S., Biancale, R., Marty, J. -C., Pérosanz, F., et al. (2007). Temporal gravity field models inferred from GRACE data. *Advances in Space Research*, *39*(10), 1620–1629.

Marengo, J. A., Tomasella, J., Soares, W., Alves, L. M., & Nobre, C. (2011). Extreme climatic events in the Amazon basin: Climatological and hydrological context of recent floods. *Theoretical and Applied Climatology*, *107*(1–2), 73–85. http://dx.doi.org/10.1007/s00704-011-0465-1.

Margat, J. (2007). Great aquifer systems of the world. In L. Chery, & G. de Marsily (Eds.), *Aquifer systems management: Darcy's legacy in a world of impending water* (pp. 105–116). Oxford, England: Taylor and Francis.

Meade, R. H., Rayol, J. M., Conceição, S. C., & Navidade, J. R. G. (1991). Backwater effects in the Amazon basin of Brazil. *Environmental Geology and Water Sciences*, *18*, 105–114.

Pereira, A., & Pacino, M. C. (2012). Annual and seasonal water storage changes detected from GRACE data in the La Plata Basin. *Physics of the Earth and Planetary Interiors*, *212–213*, 88–99. http://dx.doi.org/10.1016/j.pepi.2012.09.005.

Ramillien, G., Biancale, R., Gratton, S., Vasseur, X., & Bourgogne, S. (2011). GRACE-derived surface mass anomalies by energy integral approach. Application to continental hydrology. *Journal of Geodesy*, *85*(6), 313–328. http://dx.doi.org/10.1007/s00190-010-0438-7.

Ramillien, G., Bouhours, S., Lombard, A., Cazenave, A., Flechtner, F., & Schmidt, R. (2008). Land water storage contribution to sea level from GRACE geoid data over 2003–2006. *Global and Planetary Change*, *60*(3–4), 381–392. http://dx.doi.org/10.1016/j.gloplacha.2007.04.002.

Ramillien, G., Famiglietti, J. S., & Wahr, J. (2008). Detection of continental hydrology and glaciology signals from GRACE: A review. *Surveys in Geophysics*, *29*, 361–374. http://dx.doi.org/10.1007/s10712-008-9048-9.

Ramillien, G., Frappart, F., Cazenave, A., & Güntner, A. (2005). Time variations of land water storage from the inversion of 2-years of GRACE geoids. *Earth and Planetary Science Letters*, *235*(1–2), 283–301. http://dx.doi.org/10.1016/j.epsl.2005.04.005.

Ramillien, G., Frappart, F., Güntner, A., Ngo-Duc, T., Cazenave, A., & Laval, K. (2006). Time-variations of the regional evapotranspiration rate from Gravimetry Recovery And Climate Experiment (GRACE) satellite gravimetry. *Water Resources Research*, *42*, W10403. http://dx.doi.org/10.1029/2005WR004331.

Ramillien, G., Seoane, L., Frappart, F., Biancale, R., Gratton, S., Vasseur, X., et al. (2012). Constrained regional recovery of continental water mass time-variations from GRACE-based geopotential anomalies over South America. *Surveys in Geophysics*, *33*, 887–905. http://dx.doi.org/10.1007/s10712-012-9177-z.

Richts, A., Struckmeier, W. F., & Zaepke, M. (2011). WHYMAP and the groundwater resources map of the world 1:25,000,000. In J.A.A. Jones (Ed.), *Sustaining Groundwater Resources: A Critical Element in the Global Water Crisis* (pp. 159–173). Netherlands: Springer. doi: http://dx.doi.org/10.1007/978-90-3426-7_10.

Rodell, M., Chen, J., Kato, H., Famiglietti, J. S., Nigro, J., & Wilson, C. (2007). Estimating groundwater storage changes in the Mississippi River basin (USA) using GRACE. *Hydrogeology Journal*, *15*(1), 159–166.

Rodell, M., Famiglietti, J. S., Chen, J., Seneviratne, S. I., Viterbo, P., Holl, S., et al. (2004). Basin scale estimates of evapotranspiration using GRACE and other observations. *Geophysical Research Letters*, *31*(20), L20504.

Rowlands, D. D., Luthcke, S. B., Klosko, S. M., Lemoine, F. G. R., Chinn, D. S., McCarthy, J. J., et al. (2005). Resolving mass flux at high spatial and temporal resolution using GRACE intersatellite measurements. *Geophysical Research Letters*, *32*, L04310. http://dx.doi.org/10.1029/2004GL021908.

Rowlands, D. D., Luthcke, S. B., McCarthy, J. J., Klosko, S. M., Chinn, D. S., Lemoine, F. G., et al. (2010). Global mass flux solutions from GRACE: A comparison of parameter estimation strategies — Mass concentrations versus Stokes coefficients. *Journal of Geophysical Research*, *115*, B01403. http://dx.doi.org/10.1029/2009JB006546.

Salvia, M., Grings, F., Ferrazzoli, P., Barraza, V., Douna, V., Perna, P., et al. (2011). Estimating flooded area and mean water level using active and passive microwaves: The example of Parana River Delta floodplain. *Hydrology and Earth System Sciences*, *15*, 2679–2692. http://dx.doi.org/10.5194/hess-15-2679-2011.

Schmidt, R., Flechtner, F., Meyer, U., Neumayer, K. -H., Dahle, Ch., Koenig, R., et al. (2008). Hydrological signals observed by the GRACE satellites. *Surveys in Geophysics*, *29*, 319–334. http://dx.doi.org/10.1007/s10712-008-9033-3.

Seitz, F., Schmidt, M., & Shum, C. K. (2008). Signals of extreme weather conditions in Central Europe in GRACE 4-D hydrological mass variations. *Earth and Planetary Science Letters*, *268*(1–2), 165–170.

Strassberg, G., Scanlon, B. R., & Rodell, M. (2007). Comparison of seasonal terrestrial water storage variations from GRACE with groundwater-level measurements from the High Plains Aquifer (USA). *Geophysical Research Letters*, *34*, L14402. http://dx.doi.org/10.1029/2007GL030139.

Syed, T. H., Famiglietti, J. S., & Chambers, D. (2009). GRACE-based estimates of terrestrial freshwater discharge from basin to continental scales. *Journal of Hydrometeorology*, *10*(1). http://dx.doi.org/10.1175/2008JHM993.1.

Tapley, B. D., Bettadpur, S., Ries, J. C., Thompson, P. F., & Watkins, M. (2004). GRACE measurements of mass variability in the Earth system. *Science*, *305*, 503–505.

Tomasella, J., Borma, L. S., Marengo, J. A., Rodriguez, D. A., Cuartas, L. A., Nobre, C. A., et al. (2011). The droughts of 1996–1997 and 2004–2005 in Amazonia: hydrological response in the river main-stem. *Hydrological Processes*, *25*, 1228–1242. http://dx.doi.org/10.1002/hyp.7889.